Chinese Chemical Letters 37 (2026) 112403

Contents lists available at ScienceDirect

Chinese Chemical Letters

journal homepage: www.elsevier.com/locate/cclet

Supramolecular xanthium-like nanoreactor integrating photothermal effect, fenton reaction, and chemotherapy for targeted antitumor

Chaojia Luo[a,1], Hongxia Wang[a,1], Jie Yu[a,*], Yan Zhao[a,*], Yong Chen[b,*]

[a] College of Chemistry and Chemical Engineering, Yunnan Key Laboratory of Modern Separation Analysis and Substance Transformation, Yunnan Normal University, Kunming 650500, China
[b] College of Chemistry, State Key Laboratory of Elemento-Organic Chemistry, Nankai University, Tianjin 300071, China

ARTICLE INFO

Article history:
Received 30 August 2025
Revised 30 December 2025
Accepted 12 January 2026
Available online 12 January 2026

Keywords:
Cyclodextrin
Supramolecular assembly
Nanoreactor
Metal-organic frameworks
Synergistic anticancer

ABSTRACT

Herein, we report a xanthium-like multicomponent supramolecular assembly with target and effective anticancer ability, which integrates photothermal therapy (PTT), chemodynamic therapy (CDT), and chemotherapy. The ferrocene-modified iron-based metal-organic frameworks (Fc-MIL-88B) act as the core-carrier to effectively doped photothermal reagent gold nanoparticles (Au) and encapsulate the model drug emodin, then further bind with the biotin-modified cyclodextrin (Bio-PE-CD) as the targeting "thorns" for cancer cells, ultimately forming the nanoreactor Fc-MIL-88B@Au@emodin@Bio-PE-CD. Notably, the supramolecular reactor not only exhibits tumor microenvironment-responsive disassembly performance to release anticancer drugs but also provides an abundant Fe source for intracellular Fenton reaction to produce hydroxyl radicals, then cooperating with the photothermal effect of gold nanoparticles to induce apoptosis of cancer cells. Finally, the trinity supramolecule exhibits excellent therapeutic efficacy and biosafety at the cellular and *in vivo* levels, providing a novel strategy for the development of synergistic antitumor nanoplatforms.

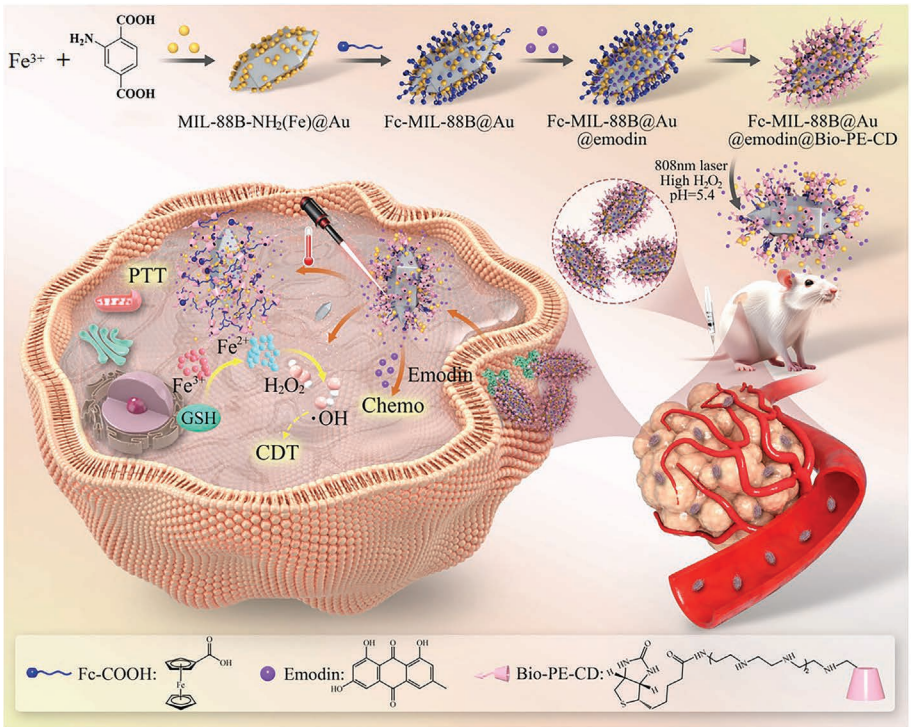
© 2026 Published by Elsevier B.V. on behalf of Chinese Chemical Society and Institute of Materia Medica, Chinese Academy of Medical Sciences.

Although many antitumor methods have been developed, including photodynamic [1], photothermal [2,3], chemotherapy [4,5], immunotherapy [6], and chemodynamic therapy [7], these therapeutic approaches inevitably have some shortcomings, and it is difficult to achieve precise targeted therapy. Among them, photothermal therapy (PTT) has received extensive attention due to its advantages of high specificity, good biocompatibility, non-invasiveness, and good selectivity. However, heat shock proteins will be activated during photothermal therapy, resulting in increased thermal tolerance of cancer cells and reduced therapeutic efficacy of PTT [8]. Nevertheless, the increased temperature in tumor can significantly improve the efficiency of Fenton or Fenton-like reactions in chemodynamic therapy [9] and promote the release of anticancer drugs in drug delivery systems [10]. Therefore, if PTT, chemotherapy, and CDT are integrated into one supramolecular platform, the efficient synergistic anticancer therapy should be realized.

To this end, the supramolecular assembly strategies provide a new development approach for the construction of a multifunctional antitumor nanoplatform. Iron-based metal-organic frameworks (Fe-MOFs) possess three-dimensional (3D) framework structures with microporous channels and cages [11–13], endowing unique advantages such as large specific surface area, high porosity, and good biocompatibility, which are beneficial to load drugs, nanozymes, and photothermal effect nanoparticles, then serve as nanocarriers in the drug delivery platform. Yet, the MOF nanocarriers still face problems such as single stimulus response, early leakage of loading drugs, and less controllability [14]. On the other hand, cyclodextrins (CDs) have hydrophobic cavity and hydrophilic hydroxyl group, which can not only bind with drugs as guests by dynamic and reversible host-guest interaction to achieve responsive drug release [15–17], but also graft specific targeting units to give macrocyclic supramolecular targeting delivery systems. Therefore, the combination of Fe-MOFs and CDs building blocks through a supramolecular assembly strategy can exert individual functionalities, mutual complementarity, and synergistic effects. Among many guest molecules that can be selectively and strongly bonded by cyclodextrins, ferrocene derivatives can be included by β-CD at a 1:1 stoichiometric ratio, giving a strong binding constant up to 10^3 L/mol [18,19], and their binding behavior exhibits re-

* Corresponding authors.
E-mail addresses: yujie5977@126.com (J. Yu), zhaooyann@163.com (Y. Zhao), yongchen@nankai.edu.cn (Y. Chen).
[1] These authors contributed equally to this work.

https://doi.org/10.1016/j.cclet.2026.112403
1001-8417/© 2026 Published by Elsevier B.V. on behalf of Chinese Chemical Society and Institute of Materia Medica, Chinese Academy of Medical Sciences.



Scheme 1. Supramolecular xanthium-like nanoreactor for synergistic antitumor therapy.

dox responsiveness. Additionally, the ferrocene derivatives possess excellent Fenton effect due to abundant Fe^{2+}, generating reactive oxygen species (ROS) with cancer cell toxicity [20,21]. Therefore, ferrocene could be served as the functional supramolecular linker to integrate CD and MOF to form tumor microenvironment-responsive supramolecular platform.

In this work, supramolecular cascade assembly strategy was employed to construct antitumor nanoreactors, in which, MIL-88B (Fe) acted as the carrier of photothermal gold nanoparticles (Au NPs) and antitumor drug emodin, then grafted with the supramolecular linker ferrocenecarboxylic acid (Fc) to give Fc-MIL-88B@Au@emodin, further bonded with targeting agent biotin functionalized β-cyclodextrin (Bio-PE-CD) to construct Fc-MIL-88B@Au@emodin@Bio-PE-CD by multi-noncovalent interactions (Scheme 1). Particularly, besides the disassembly releasing drugs from supramolecules responsive to the tumor microenvironment, the supramolecular linker in nanoreactors can catalyze the endogenous H_2O_2 to produce ·OH and Fe^{3+} by the Fenton reaction, and then the generated Fe^{3+} will react with GSH to form Fe^{2+}, achieving the oxidation/reduction cycle in cancer cells. Finally, the antitumor efficacy of nanoreactors with photothermal, chemodynamic, and chemotherapy functions was evaluated by *in vitro* and *in vivo* experiments.

Firstly, PVP-stabilized Au NPs was selected as the photothermal agent of the nanoreactor and synthesized by the reported method [22]. After centrifugation, the obtained wine-red solution gives light-path from the Tyndall effect (Fig. S1 in Supporting information), manifesting the nanoparticles existing in the solution [23]. The characteristic absorption peak of Au NPs was observed at 521 nm in UV–vis spectra (Fig. S2 in Supporting information) [24]. Fig. 1a shows that uniform spherical nanoparticles with a diameter of 20 nm were found in transmission electron microscopy (TEM) images, which was also consistent with the particle size (23 nm) tested from dynamic light scattering (DLS) experiments (Fig. 1g). Next, the Au nanoparticles were mixed up with $FeCl_3$ and 2-aminoterephthalic acid, then went through hydrothermal synthesis to prepare MOFs doped Au NPs (MIL-88B@Au). In TEM picture (Fig. 1b), MIL-88B@Au exhibits a regular biprism morphology with small nanoparticles, preliminarily suggesting Au NPs doped into MOF; the solution particle size of MIL-88B@Au is measured to be 187 nm (Fig. 1g). In addition, Energy dispersive scanning (EDS) further confirmed that the MOF carrier contained Au (Fig. S3 in Supporting information). The supramolecular linker ferrocene derivative (Fc) was grafted on the surface of nanocarriers by the condensation reaction between ferrocene carboxylic acid (Fc-COOH) and the amino group on MIL-88B@Au. The morphology of MIL-88B@Au is almost unchanged after modification with the linker Fc (Fig. 1c), but the particle size was increased to 257 nm (Fig. 1g). In the UV–vis spectrum of Fc-MIL-88B@Au (Fig. S4 in Supporting information), the characteristic absorption peak of FC was observed at 263 nm, indicating the Fc unit was introduced in the nanocarrier. Compared with MIL-88B@Au, the characteristic diffraction peak of Au-doped MOFs still exists in Fc-MIL-88B@Au (Fig. S5 in Supporting information), manifesting the modification of the carrier surface does not change the original crystal structure. The element valence and chemical bonds in Fc-MIL-88B@Au were analyzed by X-ray photoelectron spectroscopy (XPS). Significant signals of Fe, C, N, O, and Au elements were detected in the full spectrum of Fc-MIL-88B@Au (Fig. 1e). Two peaks were found at 399.3 eV and 400.5 eV in the N 1s spectrum (Fig. S6a in Supporting information), which were assigned to the C–N and O=C–N bonds, respectively, and further confirmed the successful introduction of Fc [25]. The characteristic peaks of Fe^{2+} and Fe^{3+} were found at the range of 709.5–713.0 eV and 723–726.5 eV (Fig. S6c in Supporting information), which proved that Fc was indeed connected to the nanocarriers.

Subsequently, emodin was selected as the anticancer model drug (Fig. S7 in Supporting information) to investigate the drug loading capacity of Fc-MIL-88B@Au. The emodin was added and mixed with the solution of carrier Fc-MIL-88B@Au, then shaken and oscillated by laboratory shaker to construct Fc-MIL-88B@Au@emodin. The UV–vis spectrum (Fig. S8 in Supporting in-

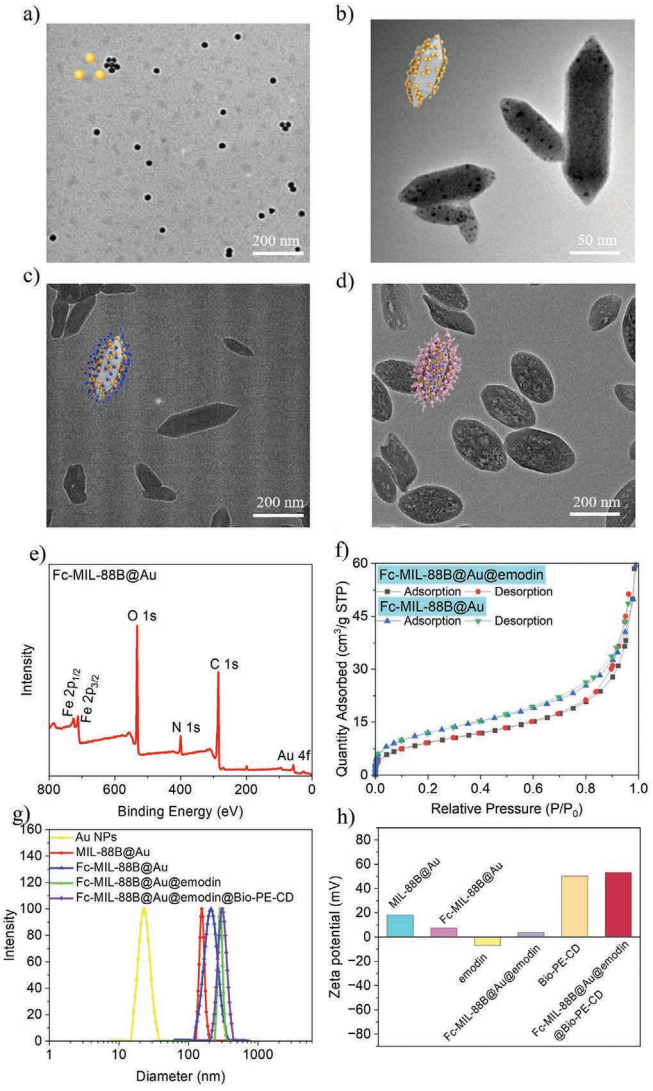


Fig. 1. TEM images of (a) Au NPs, (b) MIL-88B@Au, (c) Fc-MIL-88B@Au, and (d) Fc-MIL-88B@Au@emodin@Bio-PE-CD. (e) XPS spectrum of Fc-MIL-88B@Au. (f) Nitrogen adsorption-desorption isotherms of Fc-MIL-88B@Au@emodin and Fc-MIL-88B@Au. (g) DLS diagram of Au NPs, MIL-88B@Au, Fc-MIL-88B@Au, Fc-MIL-88B@Au@emodin, and Fc-MIL-88B@Au@emodin@Bio-PE-CD. (h) Zeta potential of MIL-88B@Au, Fc-MIL-88B@Au, emodin, Fc-MIL-88B@Au@emodin, Bio-PE-CD, and Fc-MIL-88B@Au@emodin@Bio-PE-CD.

formation) shows that the characteristic absorption peak of emodin at 466 nm was observed in Fc-MIL-88B@Au@emodin, indicating the model drug was encapsulated by the nanocarriers. At the same time, after loading emodin, the specific surface area and pore size of Fc-MIL-88B@Au decreased from 60 cm^3/g and 11.13 nm to 50 cm^3/g and 8.42 nm, respectively (Fig. 1f), the particle size increased from 257 nm to 285 nm (Fig. 1g), manifesting emodin was successfully loaded to the nanocarriers. After optimizing the substance ratio of 1:1 and the drug loading time of 36 h (Fig. S9 in Supporting information), the encapsulation efficiency and loading rate of Fc-MIL-88B@Au@emodin were tested as 40.9 % and 20.45 %, respectively. The biotin-modified β-cyclodextrin derivative Bio-PE-CD was synthesized (Scheme S1 in Supporting information) and assembled with Fc-MIL-88B@Au@emodin to give nanoreactor Fc-MIL-88B@Au@emodin@Bio-PE-CD by the strong host-guest interaction between the supramolecular linker (Fc-COOH) and β-cyclodextrin of Bio-PE-CD (Figs. S10 and S11 in Supporting information). After coassembly with Bio-PE-CD, the nanocarrier still gave "xanthium-like" assembly structure in TEM image (Fig. 1d),

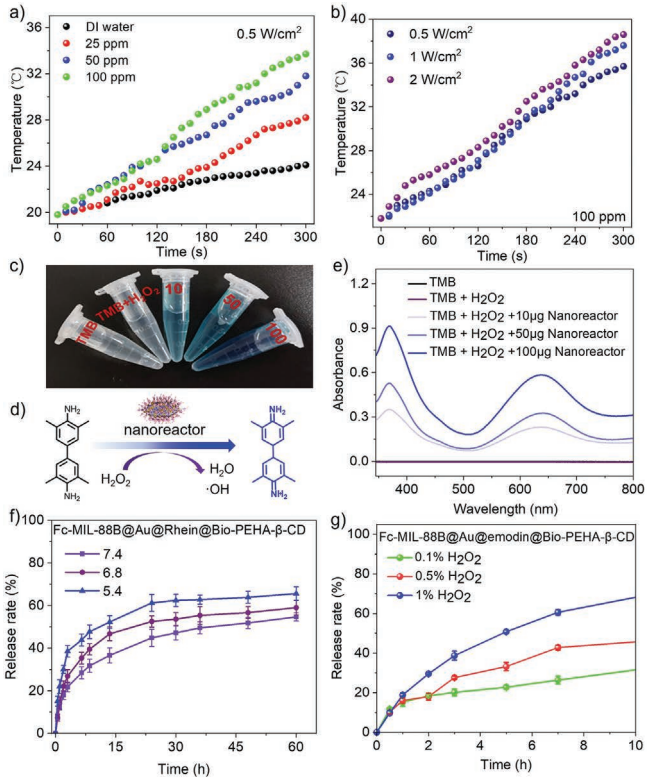


Fig. 2. (a) The temperature change curves of Fc-MIL-88B@Au@emodin@Bio-PE-CD with different concentrations under 808 nm laser irradiation. (b) The temperature change curve of Fc-MIL-88B@Au@emodin@Bio-PE-CD under different laser power density irradiation. (c) The color change of TMB solution (pH5.4) in different concentrations of nanoreactors. (d) Validation of the mechanism of ·OH production from H_2O_2 catalyzed by nanoreactor. (e) UV–vis spectra of TMB/H_2O_2 in the presence of different concentrations of nanoreactors. The release rate of Fc-MIL-88B@Au@emodin@Bio-PE-CD at different pH (f) and H_2O_2 (g) conditions.

and the particle size increased to 305 nm (Fig. 1g); thus, the nanovalve Bio-PE-CD was successfully bonded on the surface of Fc-MIL-88B@Au@emodin. In addition, Fc-MIL-88B@Au@ emodin@Bio-PE-CD gives a positively zeta potential as +53.15 mV (Fig. 1h), which is conducive to entering the cancer cells [1]. To test the stability of nanoreactors, Fc-MIL-88B@Au@emodin @Bio-PE-CD was dispersed in ethanol for 7 days, and the measured DLS did not change significantly (Fig. S12), indicating the assembly has good stability and is suitable to act as a functional antitumor nanoplatform.

Next, photothermal, catalytic, and responsive drug-releasing properties of the nanoreactor were studied to evaluate its feasibility as the antitumor nanoreactor. Laser irradiation experiments were performed to investigate the photothermal properties of Fc-MIL-88B@Au@emodin@Bio-PE-CD. Figs. 2a and b show that the solution temperature increased with the assembly concentration and laser power density. Compared with deionized water, the solution temperature of the assembly increased by 9.7 °C after 300 s irradiation with 0.5 W/cm^2 power density, showing good photothermal performance and can be applied to photothermal antitumor. Since the assembly is rich in Fe sources, including ions and ferrocene, which can act as the catalyst for the Fenton reaction of H_2O_2 to produce ·OH, the possibility of the assembly as a nanoreactor is further verified by the 3,3′,5,5′-tetramethylbenzidine (TMB) color reaction. In Fig. 2c, the color of the TMB/H_2O_2 solution was significantly turned from colorless to deep blue in the presence of Fc-MIL-88B@Au@emodin@Bio-PE-CD, indicating the generation of ·OH in the system was concentration-dependent on the nanoreactor. Furthermore, the absorbance peak was observed at 652 nm in the

presence of nanoreactor (Fig. 2e), corresponding to the characteristic signal of TMB oxide derivatives. Based on these experiments' results, the catalytic mechanism of nanoreactors was speculated in Fig. 2d. Therefore, the constructed nanoreactors responsive to the high hydrogen peroxide microenvironment of cancer cells may exert chemodynamic therapy effects.

Additionally, the drug-releasing performance of the nanoreactor under simulated tumor conditions of low pH and high H_2O_2 was further investigated by UV–vis spectroscopy. The release experiments were performed simultaneously at different pH conditions to evaluate the pH sensitivity of the assembly. As the pH value decreased from 7.4 to 5.4 (Fig. 2f), the cumulative release rate of emodin in Fc-MIL-88B@Au@emodin@Bio-PE-CD increased from 54.64 % to 65.59 %, attributing to the pH-responsive degradation ability of MOF (Fig. S13 in Supporting information). Due to an abundant iron source, the assembly will also have a stimulus-responsive behavior to H_2O_2. With the increase of the concentration of H_2O_2 from 0.1 % to 1 %, the cumulative release rate of emodin was enhanced from 33.25 % to 70.75 % (Fig. 2g). Compared with Fc-MIL-88B@Au@emodin (Fig. S14 in Supporting information), the nanoreactor equipped with Bio-PE-CD can greatly delay the release of emodin (Fig. 2g), thus, the introduction of Bio-PE-CD effectively prevents the early leakage of drugs under the same conditions. Therefore, the constructed supramolecular nanoreactor not only has good photothermal properties but also exhibits multi-stimuli responsiveness to the tumor microenvironment, showing extensive anticancer application potential.

The confocal laser scanning microscopy (CLSM) experiment was performed to investigate the uptake of Fc-MIL-88B@Au@emodin@Bio-PE-CD by cancer cells (HepG2). The model drug emodin was replaced by DOX with better fluorescence performance to facilitate the investigation of the intracellular localization of the nanoreactors. Compared to free DOX (Fig. S15 in Supporting information), the Fc-MIL-88B@Au@DOX@Bio-PE-CD gave more bright fluorescence signal in cells, which was ascribed to the introduced target unit Bio-PE-CD endowing nanoreactor with excellent tumor cell targeting ability [26], and also was conducive to the enrichment of drugs and Au NPs at the tumor site, thereby benefiting to enhance the synergistic anticancer activity. In addition, 2′,7′-dichlorofluorescein diacetate (DCFH-DA) was used as the detection reagent [27] to determine the generation of ROS in tumor cells in the presence of the nanoreactor. In Fig. 3a, Fc-MIL-88B@Au@emodin@Bio-PE-CD gave brighter green fluorescence than the control and ROS-UP groups, indicating the nanoreactor could spontaneously catalyze the Fenton reaction to generate ·OH under the conditions of tumor cells with normal temperature and no light, which is conducive to enhancing the therapeutic effect of CDT.

The synergistic anticancer activity of the constructed supramolecular nanoreactor was evaluated by cell experiments. The cytotoxicity of Fc-MIL-88B@Au@emodin@Bio-PE-CD, Fc-MIL-88B@Au@emodin@Bio-PE-CD+Laser, Fc-MIL-88B@Au@Bio-PE-CD, Fc-MIL-88B@Au@Bio-PE-CD+Laser and free emodin for tumor cells (HepG-2, MCF-7) and normal cells (L02) was studied by CCK8 method. Fig. 3b show that when the concentration of the assembly in the Fc-MIL-88B@Au@emodin@Bio-PE-CD + Laser group was 100 μg/mL (emodin in the assembly was 24.23 μg/mL), the survival rates of HepG-2 cells tested was 13.16 %. Especially, with the increase of concentration, the survival rate of the HepG-2 cells in the Fc-MIL-88B@Au@Bio-PE-CD group was also decreased from 94.18 % to 77.06 %, attributing to the Fenton reaction was activated by nanoreactors to give highly toxic ·OH, leading to the apoptosis of tumor cells. After combing laser irradiation (Fc-MIL-88B@Au@Bio-PE-CD+Laser group), the survival rate of HepG-2 cells further decreased to 46.82 %, which should be ascribed to the photothermal effect of Au NPs and its promoting effect on the

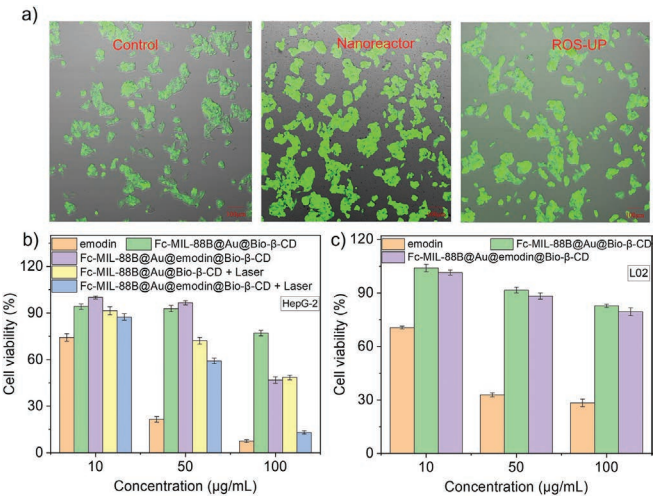


Fig. 3. (a) The DCFH-DA probe was used to detect the fluorescence intensity of HepG-2 cells after incubation with culture medium, nanoreactor, and ROS-UP (ROS induced drugs), respectively. The cell viability of (b) HepG-2 and (c) L02 incubated with different concentrations of emodin, Fc-MIL-88B@Au@Bio-PE-CD, Fc-MIL-88B@Au@emodin@Bio-PE-CD, Fc-MIL-88B@Au@Bio-PE-CD+Laser, Fc-MIL-88B@Au@emodin@Bio-PE-CD+Laser after 48 h.

Fenton reaction [28], then achieving synergistic efficient anticancer activity. Furthermore, the nanoreactor also exhibited the best apoptosis ability for MCF-7 under laser irradiation (Fig. S16 in Supporting information). For normal cells, the survival rate of L02 cells was tested to be 28.39 % with the addition of free emodin (Fig. 3c). However, the supramolecular nanoreactor gives satisfactory survival rate of up to 79.45 %, which effectively reduces the toxicity of antitumor drugs and shows good biosafety.

The biosafety of Fc-MIL-88B@Au@emodin@Bio-PE-CD was further evaluated by the hemolysis test. In Fig. S17 (Supporting information), the hemolysis rate of the assembly (1 mg/mL) was tested as 2.76 %, which was in the range of biosafety applications (<5 %) [29], showing good biosafety and intravenous administration feasibility. We also conducted more experiments to further verify the biosafety of the assembly on tumor-bearing mice. The animal usage and experimental procedures were approved by the Animal Experiment Center Committee of Yunnan University (YNU20241005), and all experimental protocols and operation procedures were performed in accordance with relevant guidelines. The tumor tissues and main organs (heart, liver, spleen, lung, and kidney) of mice in each group were taken out, and then histological analysis was performed by H&E staining. As shown in Fig. S18 (Supporting information), the images of H&E-stained tumor sections showed that the Fc-MIL-88B@Au@ emodin@Bio-PE-CD+laser group gave significant tissue damage and typical pathological features under laser irradiation, confirming its significant tumor ablation effect. Compared with nanoreactor+Laser samples, the other treatment groups only caused partial tumor tissue destruction and necrosis, showing relatively limited therapeutic effect. Especially, there were no obvious pathological changes in the heart, liver, spleen, lung, and kidney of mice in the nanoreactor and nanoreactor+Laser groups, indicating the fabricated supramolecular platform had a significant antitumor effect and had no obvious toxic and side effects on normal tissues.

The synergistic CDT/PTT/chemotherapy antitumor effect of nanoreactor was further explored by the *in vivo* experiments. Compared with the control group (PBS, Fig. S19 in Supporting information), no significant weight loss was observed in HCC1806 tumor-bearing mice treated with Fc-MIL-88B@Au@emodin@Bio-PE-CD and Fc-MIL-88B@Au@emodin@Bio-PE-CD+Laser for 14 days, indicating that the assemblies had good biocompatibility in mice. After 14-days of antitumor treatment (Fig. 4a), rapid tumor growth

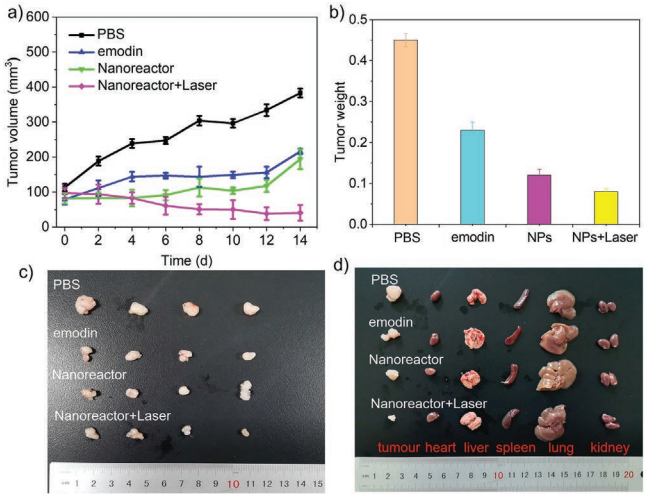


Fig. 4. The tumor volumes (a) and weight (b) of HCC1806 tumor-bearing mice with different antitumor therapy treatment at different times (data are presented as mean ± standard deviation (SD) ($n = 5$)). (c) Tumor images and (d) representative tumor and main organ tissue images dissected from tumor-bearing mice.

was observed in the PBS group, and the tumor volume increased from 113 mm^3 to 383 mm^3. Tumor volume in emodin and Fc-MIL-88B@Au@emodin@Bio-PE-CD groups was increased 2.7 and 2.3 times, respectively, showing the inhibition of tumor growth ability. However, Fc-MIL-88B@Au@emodin@Bio-PE-CD+Laser group leads to the tumor volume decreased to 41 mm^3, giving satisfactory therapeutic effect. After the antitumor treatment, the tumors and organs removed from the mice were photographed and weighed (Fig. 4b). Both the tumor volume and weight of the mice in nanoreactor+Laser group were the smallest (Figs. 4a-c), and nondamaged organs of the mice were observed (Fig. 4d), further demonstrating the biological safety of the prepared assembly and the powerful effect of the combined multi-functional treatment method. Furthermore, the antitumor effect of the nanoreactor was verified by TUNEL staining analysis of tumor apoptosis after 14 days of treatment. As shown in Fig. S20 (Supporting information), the apoptotic cells were stained green, the normal nucleus was stained blue, and there was no obvious apoptotic marker in the PBS group. The number of TUNEL-positive cells in the Fc-MIL-88B@Au@emodin@Bio-PE-CD+Laser group was the maximum, further clarifying that the nanoreactor possesses better synergistic anticancer activity.

In conclusion, a xanthium-like nanoreactor integrating photothermal, chemodynamic, and chemotherapy was successfully fabricated by the supramolecular cascade assembly strategy. The supramolecular linker grafted iron-based metal-organic frameworks (Fc-MIL-88B) with porous 3D nanostructures could act as the carrier of a nanoreactor to load the photothermal agent gold nanoparticles and the anticancer drug emodin, and then bind with the targeted nanovalve Bio-PE-CD to the MOF surface by host-guest interaction to form the supramolecular assembly of Fc-MIL-88B@Au@emodin@Bio-PE-CD. The nanoreactor shows excellent photothermal conversion performance, high-efficiency catalytic ability for Fenton reaction, and pH/H_2O_2 stimulation response for tumor microenvironment, endowing it with photothermal, chemodynamic, and chemotherapy trinity for targeted synergistic tumor apoptosis. Finally, biological experiments have shown that supramolecular nanoreactors exhibit good biocompatibility and excellent antitumor effects in cancer cells and mice, which also provides a new path for the development of synergistic anticancer nanoplatforms.

CRediT authorship contribution statement

Chaojia Luo: Writing – original draft, Visualization, Validation, Methodology, Investigation. **Hongxia Wang:** Writing – original draft, Visualization, Validation, Investigation. **Jie Yu:** Writing – review & editing, Writing – original draft, Funding acquisition. **Yan Zhao:** Supervision, Resources, Funding acquisition. **Yong Chen:** Writing – review & editing, Validation.

Declaration of competing interest

The authors declare that they have no known competing financial interests or personal relationships that could have appeared to influence the work reported in this paper.

Acknowledgments

We thank the National Natural Science Foundation of China (No. 22461048) and Science and Technology Projects of Yunnan Province University Service Key Industry (No. FWCY-ZNT2024010) for financial support.

Supplementary materials

Supplementary material associated with this article can be found, in the online version, at doi:10.1016/j.cclet.2026.112403.

References

[1] D.T. Nguyen, M.J. Baek, S.M. Lee, et al., Nat. Nanotechnol. 19 (2024) 1723–1734.
[2] G.Q. Yuan, X.X. Luo, K. He, et al., Sci. Adv. 11 (2025) eadw7032.
[3] Q.Y. Ye, Y.H. Yuan, X.H. Sun, et al., Chin. Chem. Lett. 36 (2025) 110432.
[4] J.F. Shi, Y.H. Wang, Y.H. Wu, et al., ACS Appl. Mater. Interfaces 16 (2024) 7576–7592.
[5] J. Zhou, J. Gu, X. Sun, et al., Adv. Sci. 11 (2024) 2308493.
[6] D. Sun, Y.F. Zou, L. Song, et al., Acta Pharm. Sin. B 12 (2022) 378–393.
[7] D. Sun, X. Sun, X. Zhang, et al., Adv. Healthcare Mater. 13 (2024) 2400809.
[8] Q.H. Ding, H.W. Liu, L.S. Yan, et al., Angew. Chem. Int. Ed. 64 (2025) e202505911.
[9] Q. Song, Y. Zhang, H. Hu, et al., Int. J. Nanomed. 19 (2024) 11923–11940.
[10] S.B. Lee, J.M. Park, R. Park, et al., J. Control. Release 382 (2025) 113729.
[11] R. Kudarha, N. Dhas, S. Mutalik, Coord. Chem. Rev. 494 (2023) 215330.
[12] Q.F. Zhang, G.Z. Kuang, H.B. Wang, et al., Adv. Sci. 10 (2023) 2303818.
[13] W.L. Pan, Y. Tan, W. Meng, et al., Biomaterials 283 (2022) 121449.
[14] N. Kang, S.b. Son, S.H. Min, et al., Chem. Soc. Rev. 52 (2023) 3955–3972.
[15] Z. Li, Gang Li, J. Xu, et al., Adv. Mater. 34 (2022) 2109178.
[16] J. Zhou, G.C. Yu, F.H. Huang, Chem. Soc. Rev. 46 (2017) 7021–7053.
[17] C. Zhang, J. Niu, J.Q. Li, et al., Chin. Chem. Lett. 35 (2024) 108556.
[18] Y.Y. Sun, K.X. Luo, J.N. He, et al., Carbohydr. Polym. 342 (2024) 122403.
[19] Y.H. Zhang, Y. Tian, X.L. Sheng, et al., Chin. Chem. Lett. 36 (2025) 110193.
[20] G. l. Wu, X.Tan Tan, G. Chen, Q. Yang, Theranostics 15 (2025) 384–407.
[21] S.Y. Lee, J. Park, D.I. Jeong, et al., J. Controlled Release 349 (2022) 617–633.
[22] S.K. Sivaraman, S. Kumar, V. Santhanam, J. Colloid Interface Sci. 361 (2011) 543–547.
[23] L. Chen, Y. Chen, R. Zhang, Q.L. Yu, Y. Liu, ACS Nano 16 (2022) 9929–9937.
[24] D. Liu, L. Liu, F. Liu, et al., Adv. Sci. 8 (2021) 2100074.
[25] H. Wang, Z.Y. Gao, J.M. Sun, Sep. Purif. Technol. 344 (2024) 1383–5866.
[26] C.X. Yan, N. Liang, Q.A. Li, et al., Carbohydr. Polym. 216 (2019) 129–139.
[27] Y.Q. Zeng, Y.Y. He, L. Wang, et al., Phytomedicine 128 (2024) 155533.
[28] L. Yang, Y.B. Xiang, F.F. Jia, et al., Appl. Catal. B 292 (2021) 120198.
[29] M.K. Kim, J.E. Hwang, J.S. Lee, et al., ACS Appl. Mater. Interfaces 16 (2024) 32945–32956.